Applied Surface Science 283 (2013) 227–233

Contents lists available at SciVerse ScienceDirect

Applied Surface Science

journal homepage: www.elsevier.com/locate/apsusc

Antibacterial activity and reusability of CNT-Ag and GO-Ag nanocomposites

Ji Dang Kim [a], Hyosuk Yun [a], Gwui Cheol Kim [b], Chul Won Lee [a,*], Hyun Chul Choi [a,*]

[a] Department of Chemistry, Chonnam National University, Gwangju 500-757, Republic of Korea
[b] Jeonnam Nano Bio Research Center, Jeollanam-do 515-806, Republic of Korea

ARTICLE INFO

Article history:
Received 27 February 2013
Received in revised form 10 June 2013
Accepted 17 June 2013
Available online 24 June 2013

Keywords:
Carbon nanostructures
Thiolation
Ag nanoparticles
Antibacterial materials
Reusability

ABSTRACT

A facile approach to the synthesis of novel CNT-Ag and GO-Ag antibacterial materials, in which thiol groups are utilized as linkers to secure silver (Ag) nanoparticles to the CNT and GO surfaces without agglomeration, is reported. The resulting CNT-Ag and GO-Ag samples were characterized by performing TEM, XRD, Auger, XPS, and Raman measurements, which revealed that in these antibacterial materials size-similar and quasi-spherical Ag nanoparticles are anchored to the CNT and GO surfaces. The Ag nanoparticles in CNT-Ag and GO-Ag have narrow size distributions with average diameters of 2.6 and 3.5 nm respectively. The antibacterial activities of CNT-Ag and GO-Ag against *Escherichia coli* were assessed with the paper-disk diffusion method and by determining the minimal inhibitory concentrations (MICs). CNT-Ag was found to have higher antibacterial activity than the reference Ag colloid. Moreover, both CNT-Ag and GO-Ag retain more than 50% of their original antibacterial activities after 20 washes with detergent, which indicates their potential as antibacterial materials for laboratory and medical purposes.

1. Introduction

The rise in infectious diseases caused by various pathogenic bacteria and the increasing prevalence of antibiotic-resistant strains have resulted in the devotion of more and more effort to the development of effective, non-toxic, and durable antibacterial materials [1–3]. Such materials can be broadly divided into two categories according to chemical composition: organic and inorganic agents. Organic antibacterial agents have been widely utilized because of their strong inhibitory effects on bacterial growth. Nevertheless, several disadvantages, such as low thermal stability, toxicity, and short life expectancy, have limited their applications. Thus interest in inorganic agents has been growing in recent years [4–8]. Silver (Ag) and its compounds have high bactericidal activity and biocompatibility as well as a broad spectrum of antimicrobial activities against bacteria, fungi, and even viruses, and are thus among the most important antibacterial materials. Although the mechanism of the activity of Ag nanoparticles is still inexplicit [9–11], recent studies have shown that they exhibit more efficient antibacterial activity than their bulk counterparts [12–14]. However, their high surface energy makes them highly reactive and susceptible to aggregation into large particles, which results in the deterioration of their unique chemical properties and the loss of their antibacterial activities. In an effort to overcome these problems, nanocomposites composed of Ag nanoparticles dispersed on suitable substrates have been intensively studied [15–18].

Carbon nanotube (CNT) and graphene oxide (GO) nanostructures have high mechanical strength, large surface areas, good electrical conductivity, and durability under harsh conditions, and so have been extensively studied as supporting materials [19–22]. Some of these nanostructures also exhibit good catalytic behavior in various chemical reactions. Several studies of the preparation, characterization, and antibacterial activities of carbon nanostructures combined with Ag nanoparticles have recently been reported. For example, Liu et al. prepared Ag–Fe-decorated CNTs by using DC hydrogen arc discharge, and found that these CNTs exhibit good antibacterial activity against *Escherichia coli* (*E. coli*) [23]. Li et al. reported that Ag nanoparticles supported on CNTs are very stable for six months and that their bactericidal functionality is enhanced by the synergistic effects between Ag nanoparticles and CNTs under solar irradiation [24]. Tai et al. found that Ag/graphene nanocomposites exert high antimicrobial activity against Gram-positive *Staphylococcus aureus* and Gram-negative *E. coli* [25]. Meanwhile, Das et al. reported the size and shape dependence of the antibacterial activity of Ag nanoparticles on GO [26], and Ma et al. reported synergistic effects between GO and Ag nanoparticles [27]. Akhavan et al. prepared Ag nanoparticles entrapped into

* Corresponding authors. Tel.: +82 62 530 3374/3491; fax: +82 62 530 3389.
E-mail addresses: cwlee@chonnam.ac.kr (C.W. Lee), chc12@chonnam.ac.kr (H.C. Choi).

0169-4332/$ – see front matter © 2013 Elsevier B.V. All rights reserved.
http://dx.doi.org/10.1016/j.apsusc.2013.06.086

CNT arrays, and found that these nanoparticles showed a strong antibacterial activity against *E. coli* [28]. Although all of these results are encouraging with respect to the utility of carbon nanostructures in enhancing antibacterial activities, some challenges and problems remain. Since the antibacterial activity of Ag nanoparticles is strongly dependent on particle size, high dispersion and strong metal-carbon adhesion on CNT and Ag are critical factors determining their antibacterial properties. Further, there are difficulties in the preparation of highly dispersed metal nanoparticles of regular size on carbon nanostructures, due particularly to their hydrophobic nature and tendency to agglomerate. To solve these problems, non-covalent and covalent surface-modification methods, including plasma treatment, polymer wrapping, and electrochemical treatment, have been developed [29–33]. We have introduced a simple and effective method for the preparation of metal-supported carbon materials that uses thiolated carbon nanostructures; our samples were found to exhibit excellent catalytic activity in various organic and electrochemical reactions [34–37].

In the present study, CNT-Ag and GO-Ag nanocomposites were prepared by depositing Ag nanoparticles on thiolated CNT and GO surfaces. Our transmission electron microscopy (TEM) images show that size-similar and quasi-spherical nanoparticles are highly dispersed on the surface of each sample. Auger measurements revealed that the proportions of the Ag component of the CNT-Ag and GO-Ag samples are 6.1% and 5.8% respectively. The bactericidal effects of the two samples were assessed by determining the minimal inhibitory concentrations (MIC) of both samples against *E. coli*, which were found to be 0.13 and 0.5 μg/mL respectively. Both samples exhibit moderate retention of their original antibacterial activities after detergent washings. These results suggest that CNT-Ag and GO-Ag can be utilized as reusable antibacterial materials for laboratory and medical purposes.

2. Experimental

2.1. Preparation of the antibacterial materials

2.1.1. Chemicals

Multiwall carbon nanotubes (MWNTs) were obtained from Carbon Nano Tech. Co., Ltd. (South Korea). Graphite powder (<20 μm), potassium persulfate ($K_2S_2O_8$, 99.99%), phosphorus pentoxide (P_2O_5, 99.99%), potassium permanganate ($KMnO_4$, 99%), and silver nitrate ($AgNO_3$, 99%) were purchased from Sigma–Aldrich. Other reagents were of analytical grade and were used as received without further purification. All aqueous solutions were prepared with Milli-Q water (>18.2 MΩ cm) by using the Direct Q3 system (Millipore).

2.1.2. Preparation of CNT-Ag

The MWNTs were stirred in an acid solution of HNO_3 and H_2SO_4 (1:3 by volume) at 90 °C for 3 h. They were then filtered, washed with distilled water (DI), and dried in an oven at 110 °C. Thiolation was performed as follows: the acid-treated MWNTs were dispersed in THF, then NaSH aqueous solution was added, and the mixture was stirred at 50 °C for 12 h. The thiolation was confirmed by examining the XPS spectrum in the sulfur 2p region. In this study, chemical reduction was used for Ag decoration [38]. The thiolated MWNTs (0.5 g) were dispersed in DI (15 mL), to which a 0.15 M $AgNO_3$ solution (20 mL) was added under stirring. Subsequently, a 0.1 M NaOH solution was added and stirred for 20 h. The CNT-Ag product was obtained by centrifugation, washed with DI water, and then vacuum dried at 40 °C for 24 h.

2.1.3. Preparation of GO-Ag

GO was prepared from graphite powder with the modified Hummers method [39]. The obtained GO (0.5 g) and DI water (30 mL) were added to a bottle (250 mL) and ultrasonicated for 20 min. Next, NaSH (8 g) was added gradually with stirring, and the mixture was then ultrasonicated for 1 h at 40 °C. The resultant mixture was maintained under stirring for 20 h at 55 °C to produce thiol groups on the GO surfaces. The product was filtered and washed with DI water and dried under vacuum at 50 °C for 3 h. The thiolated GO powder (0.1 g) was dispersed in DI water (30 mL) by sonication for 30 min. A 0.1 M $AgNO_3$ solution (0.5 mL) was then added to the GOSH solution under stirring. Subsequently, a 0.1 M NaOH solution was added under 20 h stirring. The GO-Ag product was obtained by centrifugation, washed with DI water, and then vacuum dried at 40 °C overnight.

2.2. Characterization

TEM images were obtained with a JEM-2200FS microscope operating at 200 kV. The samples were prepared for TEM analysis on a gold grid by dip-coating in dilute solutions. The diameters of 400 decorated nanoparticles were measured by using iTEM software (Soft Imaging System GmbH). For non-symmetrical particle shapes, both the longest and shortest dimensions were measured to obtain an average diameter value. X-ray diffraction analysis was performed by using an X'Pert-Pro high-resolution X-ray diffractometer (PANalytical, Netherlands) with Cu K_α radiation (λ = 1.5406 Å). Data were collected at room temperature within the range 4–60° at increments of 0.05°. For surface chemical analysis, Auger electron spectroscopy (AES) was performed by using a PHI 700 scanning Auger nanoprobe with an incident electron energy of 10 keV. XPS analysis was conducted with a VG Multilab 2000 spectrometer (ThermoVG Scientific) in an ultra-high vacuum; this system uses an unmonochromatized Mg K_α (1253.6 eV) source and a spherical section analyzer. The accuracy of the binding energy (BE) values was ± 0.1 eV. For analysis of the XPS peaks, the C 1s peak position was set at 284.5 eV and used as the internal reference for the location of the other peaks. Raman spectra were obtained at room temperature by using a Jobin Yvon/HORIBA LabRam ARAMIS Raman spectrometer equipped with an integral BX 41 confocal microscope. The radiation from an air-cooled frequency-doubled Nd:Yag laser (532 nm) was applied as the excitation source. The amount of Ag released from the CNT-Ag or GO-Ag nanocomposite was determined by LC-inductively coupled plasma mass spectrometer (LC-ICP-MS) with Nexion 300X model (Perkin Elmer).

2.3. Evaluation of antibacterial activity

2.3.1. Paper-disk diffusion method

The paper-disk diffusion method was employed to determine the antibacterial activities of the samples. A suspension of *E. coli* [80 μL with 1×10^7 colony forming units/mL (CFU/mL)] obtained from the Korean Collection for Type Cultures (KCTC 1682) at the Korea Research Institute of Bioscience and Biotechnology was inoculated into Mueller Hinton agar (MHA) plates. Whatman filter paper discs (4 mm diameter) were placed on the inoculated plates, and 20 μL of 440 μg/mL samples were added and allowed to dry for 15 min, after which they were incubated at 37 °C for 24 h. The size of the inhibition zone was determined by using the equation

$$\text{Size of inhibition zone (in millimeters)} = [(\text{halo-diameter of specimen}) - (\text{diameter of paper disc})] \times \frac{1}{2}.$$

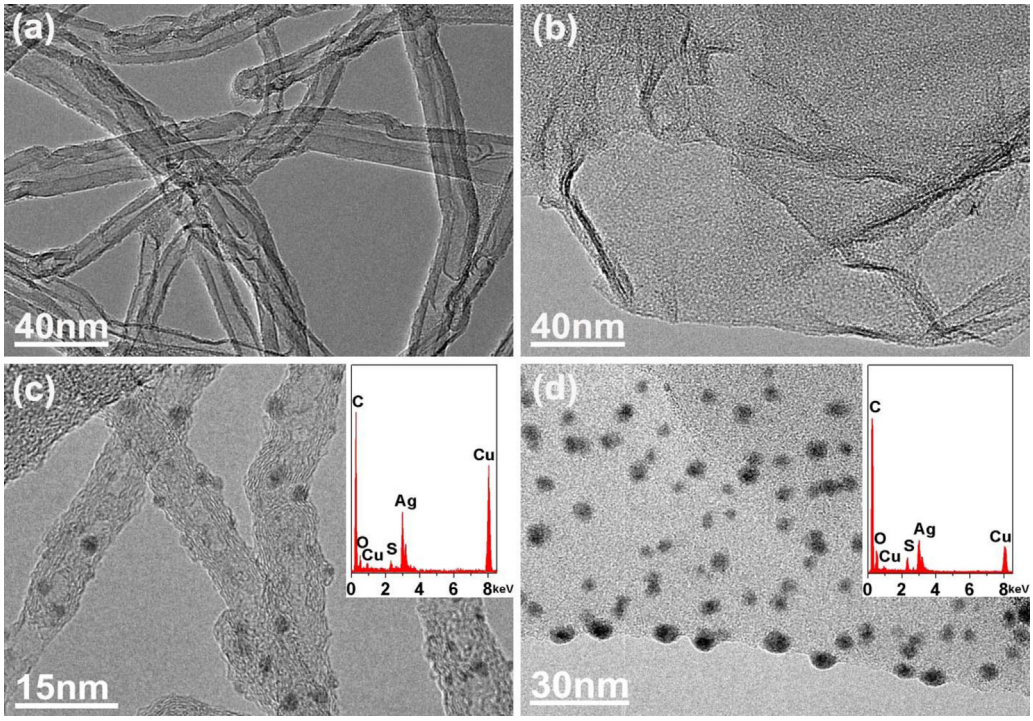

Fig. 1. (a) Transmission electron microscopy (TEM) image of thiolated CNT, (b) TEM image of thiolated GO, (c) TEM image of CNT-Ag with corresponding EDS spectrum (inset) and (d) TEM image of GO-Ag with corresponding EDS spectrum (inset).

2.3.2. Minimal inhibitory concentration (MIC) measurements

The antibacterial activities of the CNT-Ag and GO-Ag samples were determined on sterile 96-well 200 μL plates as follows. Aliquots (100 μL) of an *E. coli* suspension of 4×10^6 CFU/mL in 1% peptone were added to 100 μL sample solutions (serial two-fold dilutions in 1% peptone). After incubation for 20 h at 37 °C, each MIC was determined by visually locating the cell with no bacterial growth and the lowest concentration of the sample solution.

2.3.3. Reusability test

Samples suitable for the reusability tests were prepared by using two different procedures, autoclaving and detergent washing. In the autoclave procedure, the CNT-Ag and GO-Ag solutions were sterilized with high-pressure saturated steam at 120 °C for 20 min. Autoclaving was repeated up to five times. For the detergent-washed samples, the CNT-Ag and GO-Ag solutions were washed with 5% sodium dodecyl sulfate (SDS) in water by vortex for 1 min and centrifuged at 15,000 rpm for 5 min. The supernatant was removed immediately after centrifugation. Five (5-), 10-, 15-, and 20-times washed samples were prepared. Following the final SDS washing step, the samples were rinsed with water and then 1% peptone medium in preparation for testing for antibacterial activity.

3. Results and discussion

Fig. 1 shows typical TEM images of thiolated CNT, thiolated GO, CNT-Ag, and GO-Ag. As can be seen in Fig. 1(a), the diameters of the thiolated CNTs range from 20 to 30 nm, with a wall thickness of approximately 8 nm. Fig. 1(b) shows an image of thiolated GO with agglomerated and overlapped graphene sheets. Both the thiolated CNT and GO samples have clean surfaces. Figs. 1(c) and (d) show clearly the presence of a large number of nanoparticles anchored to the CNT and GO surfaces. The adhered nanoparticles have quasi-spherical morphologies and are uniformly dispersed. In both samples, most of the nanoparticle diameters are in the range 2–4 nm. The corresponding energy-dispersive X-ray (EDS) analyses show that the species supported on the CNT and GO surfaces is Ag [see the insets in Figs. 1(c) and (d)].

Fig. 2 shows particle-size histograms for CNT-Ag and GO-Ag. Each histogram was fitted with a Gaussian curve to obtain the particle-size distribution. The nanoparticles in CNT-Ag and GO-Ag have narrow size distributions with average diameters of 2.6 and 3.5 nm respectively. The small size and excellent dispersion of nanoparticles can elevate the bactericidal effect of antibacterial agents and reduce the required amount of expensive precious metal. Our results show therefore that thiolated carbon nanostructures are very useful for tuning the size and dispersion of metal species in metal-decorated antibacterial materials.

Fig. 3 shows the XRD patterns for thiolated CNT, thiolated GO, CNT-Ag, and GO-Ag. Thiolated CNT produces a strong (0 0 2) peak at 25.6° with a typical interlayer spacing of 0.34 nm. Thiolated GO exhibited a broad peak at 11.3° corresponding to the (0 0 2) interlayer spacing of 0.78 nm, which indicates that the ordinal structures of graphite have been destroyed and that oxygenous and thiol groups have been inserted into the interspaces. After nanoparticle deposition, four distinct diffraction peaks appear at $2\theta = 38.2°$, 44.4°, 64.5°, and 77.5°, which correspond respectively to the (1 1 1), (2 0 0), (2 2 0), and (3 1 1) crystalline planes of metallic Ag (JCPDS No. 04-0783). These observations confirm that the metallic Ag nanoparticles are effectively anchored to the thiolated CNT and GO surfaces.

Fig. 4(a) plots the Auger spectroscopic data for CNT-Ag and GO-Ag. S, C, Ag, O, and Na peaks are present in the spectra at 155, 275, 361, 520, and 998 eV, respectively. The Ag contents of the samples were estimated from the Auger peak areas and corrected according to tabulated sensitivity factors. The estimated proportions of Ag in the CNT-Ag and GO-Ag samples are approximately 6.1 and 5.8% respectively. The oxidation state of the Ag species anchored to the CNT and GO surfaces was verified with XPS measurements. Fig. 4(b) shows the Ag 3d XPS spectra for CNT-Ag, GO-Ag, and a reference Ag foil. The BEs of 368.3 eV for Ag $3d_{5/2}$ and 374.3 eV for $3d_{3/2}$ are consistent with the binding energy of the reference Ag foil. Some researchers have suggested that electron transfer from

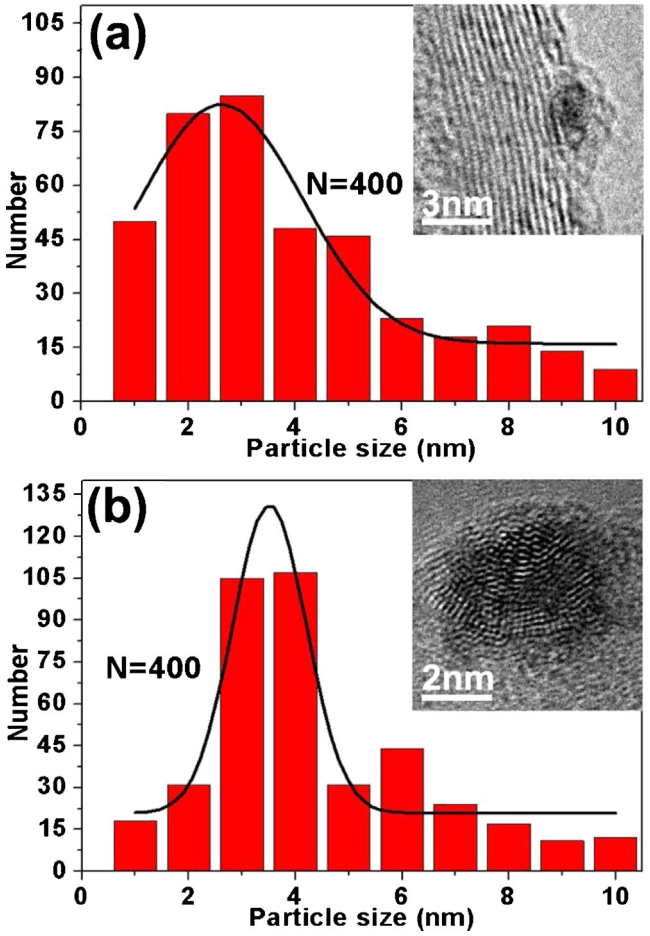

Fig. 2. Size-distribution histograms of nanoparticles in (a) CNT-Ag and (b) GO-Ag. The solid line in the histogram graphs represents a Gaussian fitting curve. The insert shows an atomic-resolved image of the deposited Ag nanoparticles.

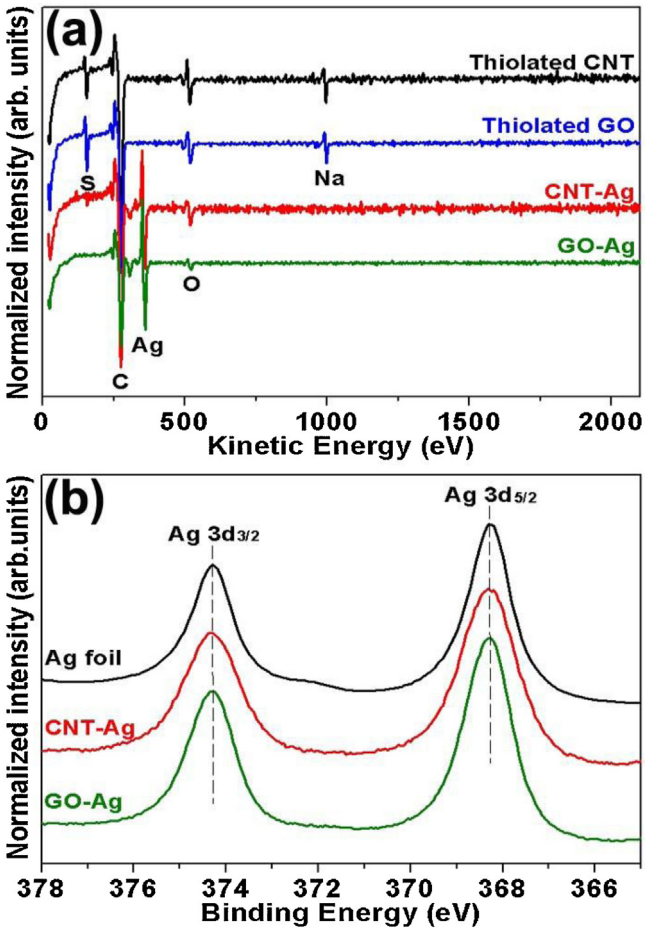

Fig. 4. (a) Auger spectra for thiolated CNT, thiolated GO, CNT-Ag, and GO-Ag, respectively and (b) Ag 3d core-level spectra for CNT-Ag, GO-Ag, and reference Ag foil, respectively.

Ag nanoparticles to GO sheets can occur during the formation of GO-Ag nanocomposites, because the work function of Ag (4.2 eV) is smaller than that of graphene (4.48 eV), which effects a shift in the BE of Ag $3d_{5/2}$ to a lower level than that of bulk Ag [40–42]. In the present study, however, no electron transfer from Ag nanoparticles to GO sheets is evident in the Ag 3d XPS spectra. Moreover, no significant changes were observed in the BEs or the intensities of the Ag core-level spectra after the exposure of the CNT-Ag and GO-Ag samples to air for three months, which demonstrates the stability of the Ag nanoparticles.

Raman spectroscopy was used to investigate the crystallinities of the CNT-Ag and GO-Ag samples. As shown in Fig. 5, the spectra consist of two bands at ~1330 cm^{-1} (D band) and 1570 cm^{-1} (G band) [43,44]. The D band is a disorder-induced feature originating

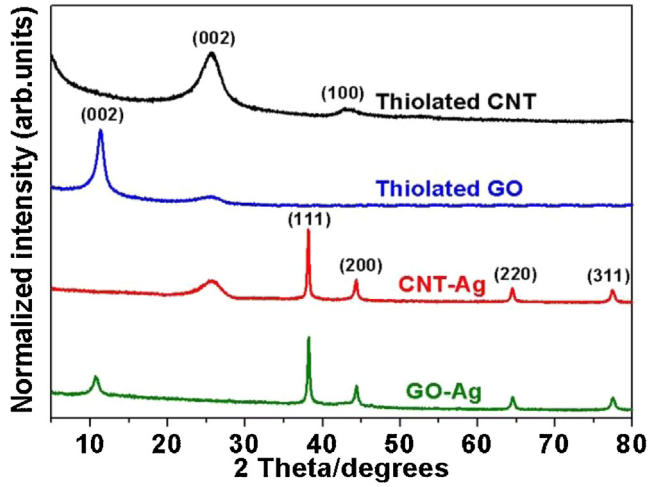

Fig. 3. XRD patterns for thiolated CNT, thiolated GO, CNT-Ag, and GO-Ag, respectively.

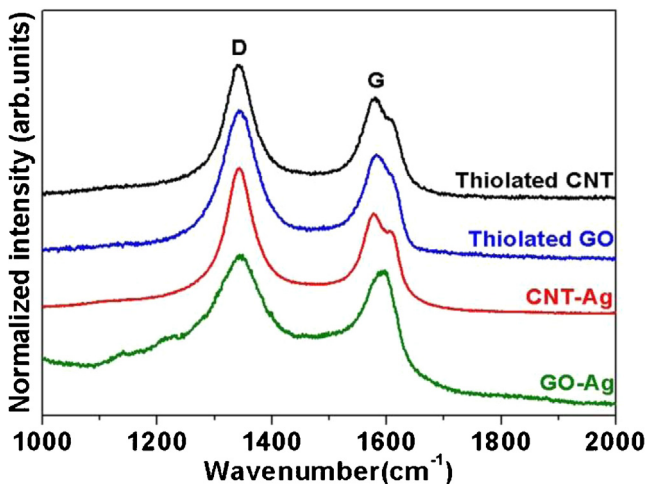

Fig. 5. Raman spectra for thiolated CNT, thiolated GO, CNT-Ag, and GO-Ag, respectively.

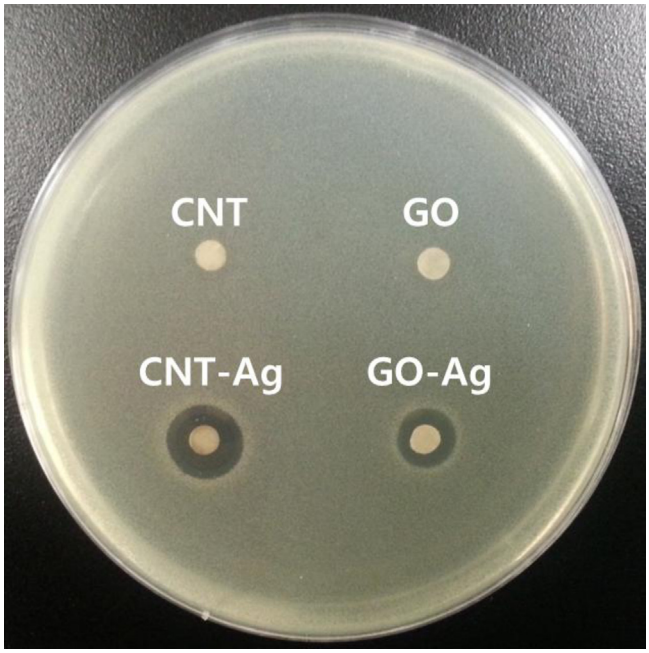

Fig. 6. Photograph of result of antibacterial test using paper-disk diffusion method against Gram-negative *E. coli* bacteria. The inhibition zone around the filter paper disk was impregnated with 440 μg/mL of samples.

from the vibrations of C atoms with dangling bonds. The G band arises from the tangential shear mode of the C atoms, which corresponds to the stretching mode on the graphite plane. The integrated intensity ratio of the D band to the G band (I_D/I_G) has a linear relation to the inverse of the in-plane crystallite dimension. The I_D/I_G values are approximately 1.28, 1.42, 1.52, and 1.23 for thiolated CNT, thiolated GO, CNT-Ag, and GO-Ag, respectively.

The antibacterial activities were initially assessed with the paper-disk diffusion method, which is widely used for quick antibiotic susceptibility determinations. As shown in Fig. 6, both CNT-Ag and GO-Ag exhibit significant inhibitory effects on *E. coli*. These results show that the antibacterial activities of the samples are mainly due to the adhered Ag nanoparticles, not the CNTs or GO. The inhibitory effects of the samples are summarized in Table 1. The reference Ag colloids have a slightly larger inhibition zone (4.3 mm) than CNT-Ag (3.5 mm) and GO-Ag (2.5 mm) at a sample concentration of 440 μg/mL, which might arise because the diffusion properties of the Ag colloids are better than those of CNT-Ag and GO-Ag in which the Ag nanoparticles are adhered to CNT or GO.

In order to obtain more precise and comprehensive data for the antibacterial activities of both samples against *E. coli*, we measured the MIC values of the nanocomposites; the results are summarized in Table 1. The MIC values are similar to previous results obtained with a bacteria growth curve method [11]. The MIC of CNT-Ag (0.13 μg/mL) is lower than that of the reference Ag colloid (0.21 μg/mL). This enhanced antibacterial activity is attributed to the high surface area of this antibacterial material, which results from the small size and excellent dispersion of the Ag nanoparticles

Table 1
Summary of antibacterial activities against Gram-negative *E. coli* bacteria.

	Ag colloid	CNT	CNT-Ag	GO	GO-Ag
Inhibition zone[a]	4.3	0	3.5	0	2.5
MIC[b]	0.21	–[c]	0.13	–[c]	0.5

[a] Measured from paper-disk diffusion method (mm).
[b] Minimal inhibitory concentration (μg/mL).
[c] not detected up to 440 μg/mL sample concentration.

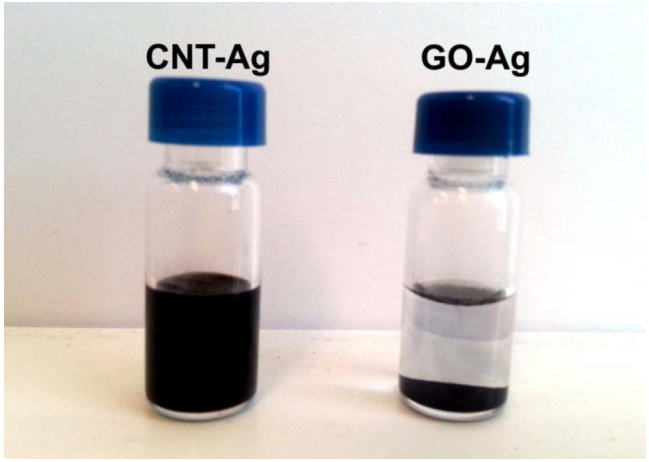

Fig. 7. Photographs of dispersion of CNT-Ag and GO-Ag in water.

on the CNT surface. However, the MIC of GO-Ag is 3.8 times higher than that of CNT-Ag, which reflects the degrees of aggregation of the two samples. CNT is a cylindrical nanostructure with pure carbon in a regular hexagonal pattern. However, GO is a layer-structured compound that is easily stacked due to the strong π–π interactions between individual nanosheets. The TEM images in Fig. 1(b) show the stacking of GOs. This difference in the chemical properties of CNT and GO means that CNT-Ag and GO-Ag have different antibacterial activities. As can be seen in Fig. 7, the dispersion of CNT-Ag in water is slightly better than that of GO-Ag, which might also result in a lower MIC value for CNT-Ag.

Carbon nanostructures are stable, inert, and multipurpose materials. Thus the reuse of silver-carbon nanostructures is possible. We tested the reusability of CNT-Ag and GO-Ag as antibacterial agents, and in particular their resistance to autoclaving and SDS washing, which are the most reliable and widely used procedures to remove bacterial contamination. SDS is an anionic detergent used in many cleaning and hygiene products in both laboratory and industry settings. We employed the paper-disk diffusion method to measure the antibacterial activities of the autoclaved and detergent-washed samples. After only a single autoclave, the antibacterial activities of both CNT-Ag and GO-Ag are approximately halved with respect to those of the non-treated samples. After a second autoclave, the antibacterial activities of both CNT-Ag and GO-Ag disappeared completely [Fig. 8(a)]. Thus certain chemical and/or physical modifications of the CNT-Ag and GO-Ag samples occur as a result of autoclaving. In contrast, the detergent-washed samples retained more than 50% of their original antibacterial activities even after 20 detergent washes [Fig. 8(b)]. To elucidate the Ag release from CNT or GO structure after each detergent washing cycle, the concentration of dissolved Ag in the sample solution was determined by LC-ICP-MS. The obtained results are summarized in Table 2. Although the values of dissolved Ag was not constant for all cycles, minor

Table 2
Amount of dissolved Ag released from CNT-Ag and GO-Ag after each detergent washing cycle.

Washing cycle	CNT-Ag		GO-Ag	
	Dissolved Ag (μg/mL)	Ag (%)[a]	Dissolved Ag (μg/mL)	Ag (%)[a]
0	<0.05	<0.02	3.0	1.9
5	<0.05	<0.02	5.2	3.3
10	<0.05	<0.02	3.8	2.4
15	<0.05	<0.02	3.8	2.4
20	<0.05	<0.02	2.7	1.7

[a] Percentage of Ag released from the total Ag (160 μg/mL) attached to CNT or GO.

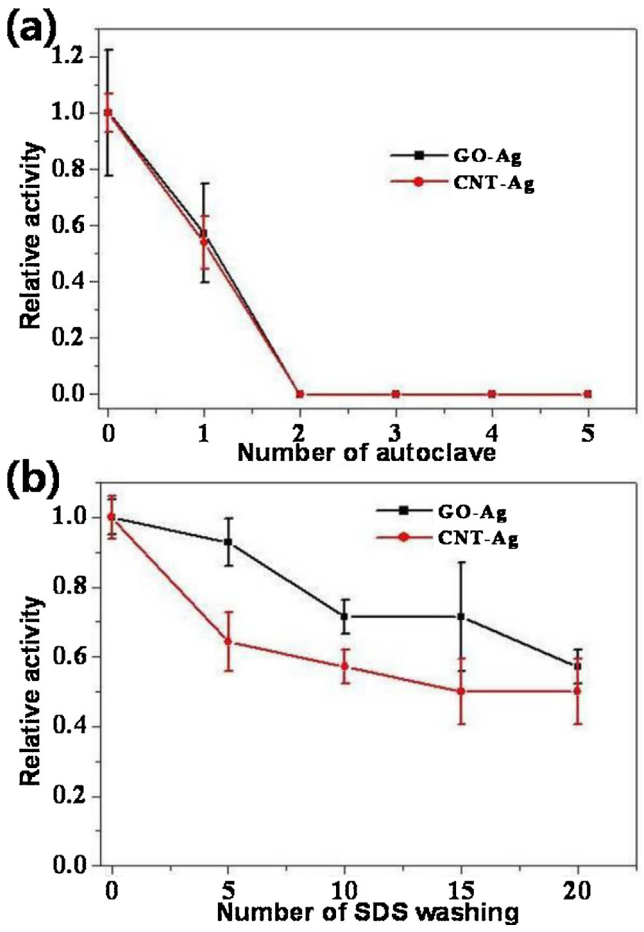

Fig. 8. Relative antibacterial activities of autoclaved and detergent-washed samples compared to their original antibacterial activities.

dissolution of less than around 3% of the total Ag was detected from the after each detergent washing cycle. Moreover, the amount of dissolved Ag was not changed by treating an acidic solution (50 mM HNO_3). This was due to the strong metal-thiol interaction. The Ag nanoparticles are linked to CNT and GO by the metal-thiol interaction, which is very strong and stable, so we believe that the metal-thiol bond is not broken by the SDS washing steps. One possible explanation for the observed decrease in antibacterial activity is that since amphipathic SDS can interact with CNT and GO the surfaces of the CNT-Ag and GO-Ag samples become partially coated with SDS molecules, which are not completely removed by the final water and 1% peptone rinse steps. The presence of an SDS coating on CNT-Ag and GO-Ag might inhibit their antibacterial activities. Additionally, there might have been some sample loss during the washing steps, as the samples were not completely precipitated by centrifugation. Investigations into the mechanism of the loss of antibacterial activity of CNT-Ag and GO-Ag are currently underway in our laboratory.

4. Conclusions

Ag nanoparticles can easily be introduced onto CNT and GO surfaces through thiolation. The size-similar and quasi-spherical nanoparticles were found to be anchored to the CNT and GO surfaces, and the synthetic CNT-Ag and GO-Ag materials were demonstrated to exhibit high antibacterial activities against Gram-negative *E. coli* bacteria. Both samples retain more than half of their original antibacterial activity after 20 detergent washes. The CNT-Ag and GO-Ag nanocomposites are therefore believed to have significant potential for use as reusable antibacterial agents for laboratory and medical purposes.

Acknowledgments

This research was supported by the Basic Science Research Program through the National research Foundation of Korea (NRF) funded by the Ministry of Education, Science and Technology (2010-0003963). Authors thank for TEM analysis from the Korea Basic Science Institute (KBSI)–Gwangju branch in Chonnam National University.

References

[1] I. Chopra, Research and development of antibacterial agents, Current Opinion in Microbiology 1 (1998) 495–501.
[2] S.B. Bataillon, P. Tattevin, M.B. Mallet, A.J. Gougeon, Emergence of resistance to antibacterial agents: the role of quaternary ammonium compounds-a critical review, International Journal of Antimicrobial Agents 39 (2012) 381–389.
[3] M.J. Hajipour, K.M. Fromm, A.A. Ashkarran, D.J.D. Aberasturi, I.R.D. Larramendi, T.R.V. Serpooshan, S.J. Parak, M. Mahmoudi, Antibacterial properties of nanoparticles, Trends in Biotechnology 30 (2012) 499–511.
[4] Z. Jing, D. Guo, W. Wang, S. Zhang, W. Qi, B. Ling, Comparative study of titania nanoparticles and nanotubes as antibacterial agents, Solid State Sciences 13 (2011) 1797–1803.
[5] H. Xia, B. Cui, J. Zhou, L. Zhang, J. Zhang, X. Guo, H. Guo, Synthesis and characterization of Fe_3O_4@C@Ag nanocomposites and their antibacterial performance, Applied Surface Science 257 (2011) 9397–9402.
[6] C. Karunakaran, V. Rajeswari, P. Gomathisankar, Enhanced photocatalytic and antibacterial activities of sol-gel synthesized ZnO and Ag-ZnO, Materials Science in Semiconductor Processing 14 (2011) 133–138.
[7] G. Gu, J. Xu, Y. Wu, M. Chen, L. Wu, Synthesis and antibacterial property of hollow SiO_2/Ag nanocomposite spheres, Journal of Colloid and Interface Science 359 (2011) 327–333.
[8] S. Jaiswal, P. McHale, B. Duffy, Preparation, rapid analysis of antibacterial silver, copper and zinc doped sot-gel surfaces, Colloids and Surfaces B 94 (2012) 170–176.
[9] J.R. Morones, J.L. Elechiguerra, A. Camacho, K. Holt, J.B. Kouri, J.T. Ramírez, M.J. Yacaman, The bactericidal effect of silver nanoparticles, Nanotechnology 16 (2005) 2346–2353.
[10] A.D. Ehre, H. Mamane, T. Belenkova, G. Markovich, A. Adin, Silver nanoparticle-*E. coli* colloidal interaction in water and effect on *E. coli* survival, Journal of Colloid and Interface Science 339 (2009) 521–526.
[11] W. Li, X. Xie, Q. Shi, H. Zeng, Y.O. Yang, Y. Chen, Antibacterial activity and mechanism of silver nanoparticles on *Escherichia coli*, Applied Microbiology and Biotechnology 85 (2010) 1115–1122.
[12] V.K. Sharma, R.A. Yngard, Y. Lin, Silver nanoparticles: green synthesis and their antimicrobial activities, Advances in Colloid and Interface Science 145 (2009) 83–96.
[13] M. Zhou, Z. Wei, H. Qiao, L. Zhu, H. Yang, T. Xia, Particle size and pore structure characterization of silver nanoparticles prepared by confined arc plasma, Journal of Nanomaterials 2009 (2009) 1–5.
[14] H.Y. Song, K.K. Ko, I.H. Oh, B.T. Lee, Fabrication of silver nanoparticles and their antimicrobial mechanisms, European Cells & Materials 11 (2006) 58.
[15] Y. Zhang, S. Zhong, M. Zhang, Y. Lin, Antibacterial activity of silver-loaded zeolite A prepared by a fast microwave-loading method, Journal of Materials Science 44 (2009) 457–462.
[16] X. Cao, M. Tang, F. Liu, Y. Nie, C. Zhao, Immobilization of silver nanoparticles onto sulfonated polyethersulfone membranes as antibacterial materials, Colloids and Surfaces B 81 (2010) 555–562.
[17] T. Angelova, N. Rangelova, R. Yuryev, N. Georgieva, R. Müller, Antibacterial activity of SiO_2/hydroxypropyl cellulose hybrid materials containing silver nanoparticles, Materials Science and Engineering: C 32 (2012) 1241–1246.
[18] B. Roy, P. Bharali, B.K. Konwar, N. Karak, Silver-embedded modified hyperbranched epoxy/clay nanocomposites as antibacterial materials, Bioresource Technology 127 (2013) 175–180.
[19] S. Iijima, Helical microtubules of graphitic carbon, Nature 354 (1991) 56–58.
[20] K.S. Novoselov, A.K. Geim, S.V. Morozov, D. Jiang, Y. Zhang, S.V. Dubonos, I.V. Grigorieva, A.A. Firsov, Electric field effect in atomically thin carbon films, Science 306 (2004) 666–669.
[21] M.J. Allen, V.C. Tung, R.B. Kaner, Honeycomb carbon: a review of graphene, Chemical Reviews 110 (2010) 132–145.
[22] D. Eder, Carbon nanotube-inorganic hybrids, Chemical Reviews 110 (2010) 1348–1385.
[23] X. Liu, L. Yu, F. Liu, L. Sheng, K. An, H. Chen, X. Zhao, Preparation of Ag–Fe-decorated single-walled carbon nanotubes by arc discharge and their antibacterial effect, Journal of Materials Science 47 (2012) 6086–6094.
[24] Z. Li, L. Fan, T. Zhang, K. Li, Facile synthesis of Ag nanoparticles supported on MWCNTs with favorable stability and their bactericidal properties, Journal of Hazardous Materials 187 (2011) 466–472.

[25] Z. Tai, H. Ma, B. Liu, X. Yan, Q. Xue, Facile synthesis of Ag/GNS-g-PAA nanohybrids for antimicrobial applications, Colloids and Surfaces B 89 (2012) 147–151.
[26] M.R. Das, R.K. Sarma, R. Saikia, V.S. Kale, M.V. Shelke, P. Sengupta, Synthesis of silver nanoparticles in an aqueous suspension of graphene oxide sheets and its antimicrobial activity, Colloids and Surfaces B 83 (2011) 16–22.
[27] J. Ma, J. Zhang, Z. Xiong, Y. Yong, X.S. Zhao, Preparation, characterization and antibacterial properties of silver-modified graphene oxide, Journal of Materials Chemistry 21 (2011) 3350–3352.
[28] O. Akhavan, M. Abdolahad, Y. Abdi, S. Mohajerzadeh, Silver nanoparticles within vertically aligned multi-wall carbon nanotubes with open tips for antibacterial purposes, Journal of Materials Chemistry 21 (2011) 387–393.
[29] M.J. O'Connell, P. Boul, L.M. Ericson, C. Huffman, Y.H. Wang, E. Haroz, C. Kuper, J. Tour, K.D. Ausman, R.E. Smalley, Reversible water-solubilization of single-walled carbon nanotubes by polymer wrapping, Chemical Physics Letters 342 (2001) 265–271.
[30] J.L. Bahr, J.P. Yang, D.V. Kosynkin, M.J. Bronikowski, R.E. Smalley, J.M. Tour, Functionalization of carbon nanotubes by electrochemical reduction of aryl diazonium salts: a bucky paper electrode, Journal of the American Chemical Society 123 (2001) 6536–6542.
[31] X. Sun, R. Li, D. Villers, J.P. Dodelet, S. Desilets, Composite electrodes made of Pt nanoparticles deposited on carbon nanotubes grown on fuel cell backings, Chemical Physics Letters 379 (2003) 99–104.
[32] D. Guo, H. Li, High dispersion and electrocatalytic properties of platinum on functional multi-walled carbon nanotubes, Electroanalysis 17 (2005) 869–872.
[33] T. Xu, J. Yang, J. Liu, Q. Fu, Surface modification of multi-walled carbon nanotubes by O_2 plasma, Applied Surface Science 253 (2007) 8945–8951.
[34] J.Y. Kim, K. Park, S.Y. Bae, G.C. Kim, S. Lee, H.C. Choi, Preparation, characterization and catalytic properties of Pd-decorated carbon nanotubes possessing different linkers, Journal of Materials Chemistry 21 (2011) 5999–6005.
[35] J.Y. Kim, Y. Jo, S. Lee, H.C. Choi, Synthesis of Pd–CNT nanocomposites and investigation of their catalytic behavior in the hydrodehalogenation of aryl halides, Tetrahedron Letters 50 (2009) 6290–6292.
[36] Y.N. Jeong, M.Y. Choi, H.C. Choi, Preparation of Pt- and Pd-decorated CNTs by DCC-activated amidation and investigation of their electrocatalytic activities, Electrochimica Acta 60 (2012) 78–84.
[37] J.D. Kim, T. Palani, M.R. Kumar, S. Lee, H.C. Choi, Preparation of reusable Ag-decorated graphene oxide catalysts for decarboxylative cycloaddition, Journal of Materials Chemistry 22 (2012) 20665–20670.
[38] D.W.H. Fam, A.I.Y. Tok, Al. Palaniappan, P. Nopphawan, Anup Lohani, S.G. Mhaisalkar, Selective sensing of hydrogen sulphide using silver nanoparticle decorated carbon nanotubes, Sensors and Actuators B 138 (2009) 189–192.
[39] N.I. Kovtyukhova, P.J. Ollivier, B.R. Martin, T.E. Mallouk, S.A. Chizhik, E.V. Buzaneva, A.D. Gorchinskiy, Layer-by-layer assembly of ultrathin composite films from micron-sized graphite oxide sheets and polycations, Chemistry of Materials 11 (1999) 771–778.
[40] I. Lopez-Salido, D.C. Lim, R. Dietsche, N. Bertram, Y.D. Kim, Electronic and geometric properties of Au nanoparticles on highly ordered pyrolytic graphite (HOPG) studied using X-ray photoelectron spectroscopy (XPS) and scanning tunneling microscopy (STM), Journal of Physical Chemistry B 110 (2006) 1128–1136.
[41] X.J. Wu, X.C. Zeng, Periodic graphene nanobuds, Nano Letters 9 (2009) 250–256.
[42] J. Li, C.-y Liu, Ag/graphene heterostructures: synthesis, characterization and optical properties, European Journal of Inorganic Chemistry 2010 (2010) 1244–1248.
[43] C. Thomsen, C. Reich, Double resonant Raman scattering in graphite, Physical Review Letters 85 (2000) 5214–5217.
[44] S. Qsswald, E. Flahaut, H. Ye, Y. Gogotsi, Elimination of D-band in raman spectra of double-wall carbon nanotubes by oxidation, Chemical Physics Letters 402 (2005) 422–427.